Microphase segregation in molten randomly grafted copolymers

Shuyan Qi and Arup K. Chakraborty
Department of Chemical Engineering, Department of Chemistry, and Material Science Division, Lawrence Berkeley National Laboratory, University of California, Berkeley, California 94720

Nitash P. Balsara
Department of Chemical Engineering, University of California, Berkeley, California 94720

(Received 4 December 2000; accepted 8 May 2001)

We study microphase ordering of molten randomly grafted copolymers (RGCs) by using a mean field theory and the replica method to calculate the quenched average. Our results illustrate that in the weak segregation limit (WSI), the optimal wave vector q^* of the lamellar phase formed by molten RGCs, has a temperature dependence different from either linear random copolymers (LRCs) or diblock copolymers (DCPs): when close, but below the microphase separation transition (MST) temperature, q^* increases sharply with decreasing temperature; then q^* gradually acquires an asymptotic value determined by the length of the branch and the average distance between branch points on the backbone. Our results are compared with recent experiments, and the effects of chain architecture on the microphase separation characteristics of RGCs are delineated. Our results suggest a new method for controlling the microphase spacing by exploiting quenched disorder. [DOI: 10.1063/1.1382856]

I. INTRODUCTION

Blends of incompatible homopolymers separate into different macroscopic phases when cooled below a certain temperature. By chemically connecting immiscible homopolymers so as to form copolymers, phase segregation is restricted to the microscopic scale and takes place at a lower temperature. Generally, different microphase separation transition (MST) temperatures and different ordered microstructures are expected for copolymers with different chain architectures and sequences. The physics of microphase ordering in copolymers with ordered sequences and different chain architectures has been studied extensively,[1,2] and many exotic microstructures with potential applications have been observed.

In recent years, there has been increasing interest in copolymers with disordered sequence distributions because they share some features with protein sequences (e.g., Refs. 3–5), and because they serve as excellent models for studying materials with frustrating quenched disorder (e.g., Refs. 6, 7). One simple example is a linear random copolymer (LRC) formed by connecting two types of segments to assemble a linear chain with a disordered sequence. In LRCs, the disordered sequence distribution is quenched, and this provides an additional source of frustration not present in copolymers with ordered sequence distributions. Although microphase ordering in this simplest polymeric system with frustrating quenched randomness has been considered by theorists,[3–10] experiments probing the phase behavior of LRCs have not been conducted because of the difficulty of synthesizing LRCs with controlled sequence statistics.

Other than LRCs, Shinozaki *et al.*[11] have studied comb copolymers which have randomly placed teeth (consisting of type-B segments) on a homogeneous backbone (consisting of type-A segments). The free energy functional is derived up to quadratic order, and the authors discuss the dependence of the structure factor in the disordered phase on chain architecture. Similar results are obtained by Werner and Fredrickson.[12] However, as mentioned in Ref. 11 and as we shall see, the quartic terms play an important role in determining the physics of microphase ordering.

Recently, polymers with disordered and well-controlled sequence statistics have become available for careful physical experiments. By a combination of anionic polymerization and selective silane-coupling,[13] a class of heteropolymers is synthesized which consists of a homopolymer backbone (A-type segments) onto which branches (B-type segments) are grafted (with each branch having the same length). The branch points on the backbone are randomly located and cannot anneal after synthesis is complete. We refer to such materials as randomly grafted copolymers (RGCs). These materials are the same as the random comb copolymers whose structure factor in the disordered phase have been studied by Shinozaki *et al.*[11] and Werner and Fredrickson.[12] Here, we shall focus on the microphase ordering transitions of RGC melts. For this reason, we derive a free energy functional up to quartic order accounting for the quenched and disordered branch point distribution. Microphase ordering in a well-characterized RGC melt, wherein the fluctuations in branch point locations are short-range correlated with a fixed mean value, is then studied. We compare these results with optical birefringence and small angle neutron scattering (SANS) experiments. In addition, we discuss the dependence of microphase ordering on parameters that define the architecture such as the backbone length, the number of branches, and the branch length. A short account of some of these calculations and experimental results has been published.[14]

This paper is organized as follows: In Sec. II, we introduce the model and develop the free energy functional. (Details of the derivation are provided in the Appendices.) In Sec. III we employ this free energy functional to investigate the phase transition from a disordered state to a lamellar state. The dependence of this phenomenon on RGC architecture is also discussed. Section IV is devoted to a comparison of the theoretical results with experimental data. Our prediction for the optimal wave vector q^* characterizing the size of the lamellar domains and the intensity at the peak of the scattering pattern compares well with the experimental results. Section V contains a short conclusion and some discussion of related issues.

II. THEORY

The system we consider consists of N_c RGC chains. Each chain has a backbone with N monomers of type-A, and has P branches with each branch having M monomers of type-B. The branch points on the backbone are randomly distributed. The positions of the branch points for a specific chain are quenched. We emphasize that each chain in the melt has a different sequence of branch points, but all sequences belong to the same statistical distribution. Specifically, the distribution we consider is one wherein the average fraction of branch points on the backbone is P/N, and the fluctuations in branch point location exhibit short-range correlations.

For the system described above, the partition function is written as

$$Z=\left\{\Pi_{i=1}^{N_c}\Pi_{j=1}^{P}\int D\mathbf{r}_i(n)D\mathbf{r}_{ij}(s)P_0[\mathbf{r}_i(n)] \times P_0[\mathbf{r}_{ij}(s)]\delta[\mathbf{r}_{ij}(0)-\mathbf{r}(\tau_{ij})]\right\}\exp[-E], \tag{1}$$

where we use k_BT as a unit for energy (k_B is the Boltzmann constant, T is temperature). $\mathbf{r}_i(n)$ and $\mathbf{r}_{ij}(s)$ are the positions of the nth monomer on the backbone of the ith chain and the sth monomer on the jth branch of the ith chain, respectively. $P_0[\mathbf{r}_i(n)]$ and $P_0[\mathbf{r}_{ij}(s)]$ ensure the connectivity of the backbones and the branches; i.e., explicitly,

$$P_0[\mathbf{r}_1(n)]=C_N\exp\left[-\frac{3}{2b^2}\int_0^N dn\left(\frac{\partial\mathbf{r}_i(n)}{\partial n}\right)^2\right],$$
$$P_0[\mathbf{r}_{ij}(s)]=C_M\exp\left[-\frac{3}{2b^2}\int_0^M ds\left(\frac{\partial\mathbf{r}_{ij}(s)}{\partial s}\right)^2\right], \tag{2}$$

where C_N and C_M are normalization constants, and b is the statistical segment length for both monomers A and B. (We ignore the difference in statistical segment length between monomer A and monomer B. This approximation simplifies the calculation without losing any essential physics.) The δ-function in Eq. (1) ensures the connectivity of the branches to specific points on the backbone. τ_{ij} are the positions of the branch points ($j=1$ to P) on the backbone of the ith chain. The distribution of τ_{ij} is random, and we shall perform a quenched average over this distribution.[15] Let us introduce the coarse-grained macroscopic densities of monomers of both types: $\rho_A(\mathbf{r})=\Sigma_{i=1}^{N_c}\int dn\,\delta[\mathbf{r}-\mathbf{r}_i(n)]$ and $\rho_B(\mathbf{r})=\Sigma_{i=1}^{N_c}\Sigma_{j=1}^{P}\int ds\,\delta[\mathbf{r}-\mathbf{r}_{ij}(s)]$. $E=E(\rho_A,\rho_B)$ is the interaction energy, and it has the form

$$E=\frac{V}{2}\int d\mathbf{r}\{-2\chi m^2(\mathbf{r})+c^2[\nabla m(\mathbf{r})]^2\}, \tag{3}$$

where c^2 is the surface tension, χ is the Flory parameter, the order parameter $m(\mathbf{r})=\xi_B\rho_A(\mathbf{r})-\xi_A\rho_B(\mathbf{r})$, with ξ_A and ξ_B being the average volume fractions of monomers A and B. We now define the entropy to be

$$S=\ln(R)=\ln\left\{\Pi_{i=1}^{N_c}\Pi_{j=1}^{P}\int D\mathbf{r}_i(n)D\mathbf{r}_{ij}(s) \times P_0[\mathbf{r}_i(n)]P_0[\mathbf{r}_{ij}(s)]\delta[\mathbf{r}_{ij}(0)-\mathbf{r}(\tau_{ij})]\right\}, \tag{4}$$

such that $Z=\exp[S-E]$. Thus the quenched average need be performed on the entropy only, and we use the replica trick to compute this average:

$$\langle S\rangle=\lim_{\sigma\to 0}\frac{\langle R^\sigma\rangle-1}{\sigma}. \tag{5}$$

Here the average is taken over the quenched distribution of τ_{ij}. Because the free energy functional is extensive with respect to the number of chains in the melt, from this point we omit the subscript i which denotes the chains, and the subsequent free energy therefore is the free energy per chain. In addition, we define the volume of a single RGC to be $V=N+PM$ (phenomenology of a lattice model). These considerations lead to

$$\langle R^\sigma\rangle=\left\langle\Pi_{\alpha=1}^{\sigma}\Pi_{j=1}^{P}\int D\mathbf{r}^\alpha(n)D\mathbf{r}_j^\alpha(s) \times P_0[\mathbf{r}^\alpha(n)]P_0[\mathbf{r}_j^\alpha(s)]\delta[\mathbf{r}_j^\alpha(0)-\mathbf{r}^\alpha(\tau_j)]\right\rangle. \tag{6}$$

We now use a mean field theory[16] to calculate $\langle R^\sigma\rangle$, i.e., we evaluate the pertinent functional integrals using the saddle point approximation to obtain the effective free energy. The quenched average over the disordered sequence is also calculated during the process. The details of this derivation are provided in the Appendices. The final form of the entropy as a functional of coarse-grained densities ρ_A and ρ_B is shown in Eq. (A17) in Appendix A.

From this point, we enforce the incompressibility condition, i.e., $\rho_A(\mathbf{r})+\rho_B(\mathbf{r})=\rho_0$, where $\rho_0=(N+PM)/V=1$. Consequently, the quadratic coefficient becomes a scalar, and terms can be combined to form one cubic and quartic coefficient. The resulting free energy density is

$$\left\langle \frac{F}{V} \right\rangle = \frac{1}{2}\int d\mathbf{q}\left[\frac{\Sigma_{i,j=1}^{2} M_{ij}(\mathbf{q})}{\det M(\mathbf{q})} - (2\chi - c^2q^2)/(N+PM)\right] m(\mathbf{q})m(-\mathbf{q}) - \frac{V}{6}\int d\mathbf{q}_1\, d\mathbf{q}_2 [\Gamma_{30}(\mathbf{q}_1,\mathbf{q}_2)(W_{11}+W_{12})_{\mathbf{q}_1}$$
$$\times (W_{11}+W_{12})_{\mathbf{q}_2}(W_{11}+W_{12})_{-\mathbf{q}_1-\mathbf{q}_2} + \Gamma_{31}(\mathbf{q}_1,\mathbf{q}_2)(W_{11}+W_{12})_{\mathbf{q}_1}(W_{11}+W_{12})_{\mathbf{q}_2}(M_{21}+M_{22})_{-\mathbf{q}_1-\mathbf{q}_2} + \Gamma_{32}(\mathbf{q}_1,\mathbf{q}_2)$$
$$\times (W_{11}+W_{12})_{\mathbf{q}_1}(W_{21}+W_{22})_{\mathbf{q}_2}(W_{21}+W_{22})_{-\mathbf{q}_1-\mathbf{q}_2} + \Gamma_{33}(\mathbf{q}_1,\mathbf{q}_2)(W_{21}+W_{22})_{\mathbf{q}_1}(W_{21}+W_{22})_{\mathbf{q}_2}$$
$$\times (W_{21}+W_{22})_{-\mathbf{q}_1-\mathbf{q}_2}] m(\mathbf{q}_1)m(\mathbf{q}_2)m(-\mathbf{q}_1-\mathbf{q}_2) - \frac{V^2}{24}\int d\mathbf{q}_1\, d\mathbf{q}_2\, d\mathbf{q}_3 [\Gamma'_{40}(\mathbf{q}_1,\mathbf{q}_2,\mathbf{q}_3)(W_{11}+W_{12})_{\mathbf{q}_1}$$
$$\times (W_{11}+W_{12})_{\mathbf{q}_2}(W_{11}+W_{12})_{\mathbf{q}_3}(W_{11}+W_{12})_{-\mathbf{q}_1-\mathbf{q}_2-\mathbf{q}_3} + \Gamma'_{41}(\mathbf{q}_1,\mathbf{q}_2,\mathbf{q}_3)(W_{11}+W_{12})_{\mathbf{q}_1}(W_{11}+W_{12})_{\mathbf{q}_2}$$
$$\times (W_{11}+W_{12})_{\mathbf{q}_3}(W_{21}+W_{22})_{-\mathbf{q}_1-\mathbf{q}_2-\mathbf{q}_3} + \Gamma'_{42}(\mathbf{q}_1,\mathbf{q}_2,\mathbf{q}_3)(W_{11}+W_{12})_{\mathbf{q}_1}(W_{11}+W_{12})_{\mathbf{q}_2}(W_{21}+W_{22})_{\mathbf{q}_3}$$
$$\times (W_{21}+W_{22})_{-\mathbf{q}_1-\mathbf{q}_2-\mathbf{q}_3} + \Gamma'_{43}(\mathbf{q}_1,\mathbf{q}_2,\mathbf{q}_3)(W_{11}+W_{12})_{\mathbf{q}_1}(W_{21}+W_{22})_{\mathbf{q}_2}(W_{21}+W_{22})_{\mathbf{q}_3}(W_{21}+W_{22})_{-\mathbf{q}_1-\mathbf{q}_2-\mathbf{q}_3}$$
$$+ \Gamma'_{44}(\mathbf{q}_1,\mathbf{q}_2,\mathbf{q}_3)(W_{21}+W_{22})_{\mathbf{q}_1}(W_{11}+W_{12})_{\mathbf{q}_2}(W_{21}+W_{22})_{\mathbf{q}_3}(W_{21}+W_{22})_{-\mathbf{q}_1-\mathbf{q}_2-\mathbf{q}_3}]$$
$$\times m(\mathbf{q}_1)m(\mathbf{q}_2)m(\mathbf{q}_3)m(-\mathbf{q}_1-\mathbf{q}_2-\mathbf{q}_3) + \frac{V}{8}\left[\int d\mathbf{q}\frac{\Sigma_{i,j=1}^{2} M_{ij}(\mathbf{q})}{\det M(\mathbf{q})} m(\mathbf{q})m(-\mathbf{q})\right]^2$$
$$+ \frac{V}{8}\left\{\left\langle\left[\int d\mathbf{q}\frac{\Sigma_{i,j=1}^{2} M_{0ij}(\mathbf{q})}{\det M_0(\mathbf{q})} m(\mathbf{q})m(-\mathbf{q})\right]^2\right\rangle - \left\langle\int d\mathbf{q}\frac{\Sigma_{i,j=1}^{2} M_{0ij}(\mathbf{q})}{\det M_0(\mathbf{q})} m(\mathbf{q})m(-\mathbf{q})\right\rangle^2\right\}, \quad (7)$$

where the matrices Γ_i and the 2×2 matrices M, M_0, and W are defined in Appendix A. Similar to the case of diblock copolymers, the quadratic coefficient,

$$\Gamma_2(q) \approx \left[\frac{\Sigma_{i,j=1}^{2} M_{ij}(\mathbf{q})}{\det M(\mathbf{q})} - (2\chi - c^2q^2)/(N+PM)\right]$$

is repulsive in the short length scale limit (large q limit):

$$\lim_{q\to\infty}\Gamma_2(q) \approx \frac{(N+PM)}{2N\times PM} b^2q^2 + c^2q^2/(N+PM)$$
$$(N \gg M \gg P \gg 1, N \sim PM), \quad (8)$$

and is attractive in the long length scale limit (small q limit):

$$\lim_{q\to 0}\Gamma_2(q) \approx \frac{18}{b^2q^2}\frac{(N+PM)^2}{N^3PM^2} \quad (N \gg M \gg P \gg 1, N \sim PM). \quad (9)$$

A detailed discussion of the quadratic coefficient is provided in Ref. 11.

The quadratic coefficient is related to the structure factor in the disordered phase. To discuss microphase ordering, cubic and quartic terms are crucial. In the next section we discuss microphase ordering based on numerical calculations with the complete free energy functional in Eq. (7).

III. THEORETICAL PREDICTIONS

A. Microphase ordering

To illustrate the essential phase behavior of this system with frustrating quenched disorder and branched architecture, we use the simplest ordered microstructure (i.e., a lamellar structure). We define

$$m(\mathbf{q}) = \frac{A}{V}[\delta(\mathbf{q}-\mathbf{G}) + \delta(\mathbf{q}+\mathbf{G})], \quad (10)$$

where $\mathbf{G}$ is the wave vector for the lamellar structure. As a result, the cubic term vanishes because the sum of the three integrated wave vectors is zero [see Eq. (7)]. The quartic terms are also simplified. Next, we obtain the equilibrium wave amplitude A and the optimal wave vector q^* by minimizing the free energy functional in Eq. (7) with respect to these parameters.

As the temperature decreases, the energetic incompatibility between the two types of segments gradually wins over the entropic mixing effect, and different segments prefer to separate into different regions. In the weak segregation limit (WSL), i.e., temperature around MST where chain stretching is weak, there are two ways in which the system can respond to the increasing energetic driving force for microphase separation. One is to increase the wave amplitude $|A|$. The other is to increase q^* at which the lamellar structure is formed. Because of the random positions of the branch points on the backbone, RGCs have the freedom to change both q^* as well as increasing $|A|$. This is what happens (Fig. 1) as the temperature goes below MST. In contrast, polymers with ordered sequences like DCPs can only change A because the block lengths set a natural length scale.

In Fig. 1 we show the optimal wave vector q^* as a function of temperature in the vicinity of the MST for the disorder to lamellar phase transition for a chain with $N=2138$, $P=16$, and $M=285$ (the reason for choosing these values is discussed below). We find that q^* sharply increases from a fixed value q_c (the optimal wave vector for density fluctuations in the disordered state) immediately below the temperature corresponding to the MST, and then acquires an asymptotic value q_f at lower temperatures. This phenomenon

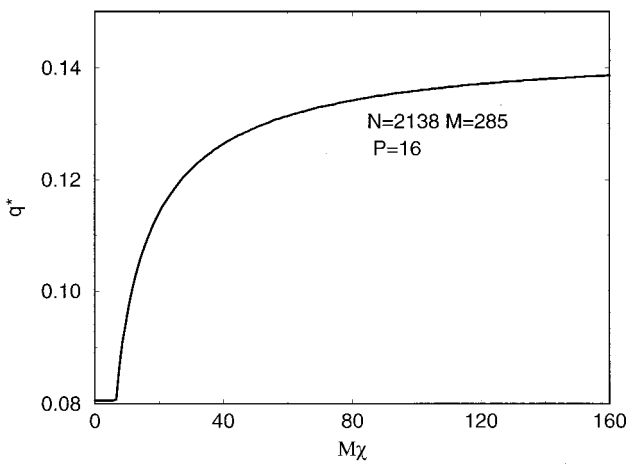

FIG. 1. The dependence of the optimal wave vector q^* on $M\chi$. The architecture parameters are chosen to be $N=2138$, $M=285$, and $P=16$.

can be understood both by analyzing the mathematical structure of the free energy functional and by physical considerations.

Let us denote the sum of the first and second quartic terms in Eq. (7) by $F_{41}(G)$, where G is the magnitude of the lamellar wave vector. $F_{41}(G)$ depends on the mean value of the sequence disorder, and not on the quenched fluctuations. It has a minimum as a function of G for fixed values of A (see Fig. 2). This minimum occurs for a value of G larger than q_c. On the other hand, the last quartic term in Eq. (7) [we denote it as $F_{42}(G)$] depends on the quenched sequence fluctuations. It is a monotonic and sharply decreasing function of G. As in the case of DCPs, the quadratic term of Eq. (7) has a well-defined minimum at $G=q_c$. It is worth noting that for linear random copolymers (LRCs), $q_c=0$. This is because there is no stoichiometric constraint associated with the connectivity of branches to branch points on the backbone for LRCs; so, the $1/q^2$ term in the quadratic coefficient for RGCs is absent for LRCs. For RGCs, in the disordered state, $A=0$ and the optimal wave vector q^* for the density

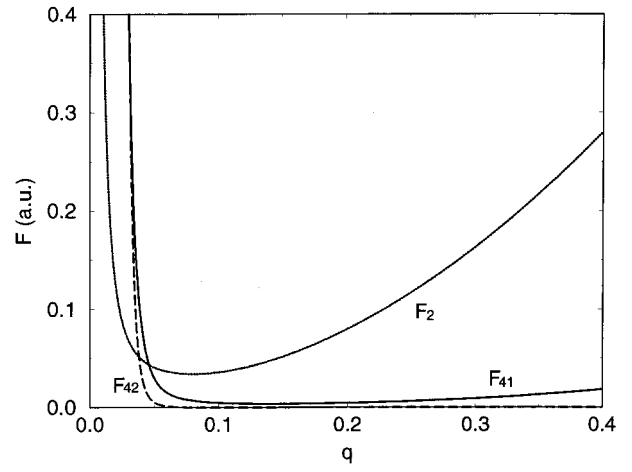

FIG. 2. The quadratic and quartic terms of free energy functional. The symbols that denote different terms in the free energy functional are discussed in the text.

fluctuations is determined by the quadratic coefficient, i.e., $q^*=q_c$. Below the MST, the optimal wave vector for microphase ordering is determined by combining the quadratic term with $F_{41}(G)$ and $F_{42}(G)$. The optimal wave vector shifts from q_c to a larger value because F_{41} and F_{42} decrease in the vicinity of $G=q_c$. As the temperature is lowered, the quartic terms gain in importance, and hence q^* shifts to continuously larger values. To answer the question of why q^* grows rapidly immediately below the MST and then becomes asymptotic at low temperature, we notice that the two quartic terms contribute differently for different values of G (see Fig. 2). F_{41} has a minimum for $G>q_c$. For large value of G, $F_{42}\approx 0$. When $G\sim q_c$, both F_{41} and F_{42} decrease quickly. This gives rise to a fast growth of q^* immediately below the MST. As q^* increases to the point of $G>q_c$ and close to the valley describing the minimum in F_{41},q^* approaches an asymptotic value in between q_c and the value of G corresponding to the minimum in F_{41}.

The dependence of q^* on temperature below MST can also be understood by considering the natural length scales that characterize the physical system under consideration. Above the MST, because entropic effects which promote mixing of the two types of segments on large scales are dominant, the characteristic length scale for concentration fluctuations ($\sim 1/q_c$) is much larger than that corresponding to the branch length or the mean value of the distance between branch points on the backbone (N/P). Immediately below the MST, the system begins to order on scales shorter than $1/q_c$. The distribution of branch points on the backbone is short-range correlated and has a fixed mean value (P/N). Statistically, this means that the number of branch points within a fixed length of the backbone satisfies the Poisson distribution, which has a very large variance at its peak position because of the long tail of the distribution for values larger than N/P. Therefore, the system can choose to order on a wide range of intrinsic length scales. Because of this freedom in choosing length scales, the system orders on progressively shorter length scales as temperature is decreased and entropic constraints become less important. However, this trend cannot continue forever. Once $1/q^*$ becomes commensurate with the branch length or the mean value of the distance between branch points on the backbone (N/P), ordering on smaller length scales is prevented because of the large entropy penalty for further squeezing the regions occupied by the branches or the backbone. This leads to q^* becoming essentially independent of temperature. The relative importance of M and N/P in determining the optimal wavevector q_f is discussed in detail below. Here we want to mention that the essential point is that q^* becomes asymptotic because a natural length scale emerges.

The rapid increase and subsequent saturation of q^* with temperature for RGCs differs from microphase separation characteristics of molten block copolymers with ordered sequences (such as DCPs) or LRCs. For DCPs, it is well-established that q^* is relatively insensitive to temperature in the vicinity of the MST, and declines with decreasing temperature at lower temperatures due to chain stretching.[17] For molten LRCs, theoretical studies predict that q^* increases below the MST and this trend continues until $1/q^*$ becomes

commensurate with segmental scales.[3,9] For random block copolymers,[18–21] a natural length scale larger than the statistical segment length does exist, viz., the length of the blocks. However, this is different from RGCs where the minimal length defining the backbone (which embodies the randomness) is still the statistical segment length. Further, for RGCs, the free energy functional is different from linear random block copolymers because of terms arising from the branched architecture. From the analysis above, it is clear that RGCs behave differently because of frustration due to the quenched sequence disorder and the existence of a natural length scale which can be much shorter than chain dimensions. The quenched sequence disorder allows RGCs the freedom to choose progressively shorter wavelength upon decreasing temperature immediately below the MST, while a system with ordered sequence (e.g., DCPs) only has fixed optimal wavelength commensurate with the sequence (without considering chain stretching). For RGCs, just below the MST, the dominant influence comes from the fluctuations in the branch point positions which compels the chain to separate into smaller domains. As the temperature is lowered further, however, a natural length scale (shorter than chain dimensions) emerges, and q^* becomes insensitive to temperature. For LRCs, the natural length scale is the monomer size. So, q_f for LRCs is practically infinity.

B. Effects of chain architecture

We shall consider the effects of chain architecture by discussing the variation of q_c and q_f with M and P. q_c corresponds to the optimal length scale of density fluctuations in the disordered state, and its variation with architectural parameters has been discussed before.[11] Here, we wish to focus on the scaling behavior of the optimal wave vector as a natural length scale begins to emerge. What value of q^* (or temperature) should we choose to study this issue? We must choose a value after the temperature window wherein q^* increases rapidly. However, satisfying this condition does not yield a precise criterion. Figure 1 shows that at the end of the regime where q^* increases rapidly with decreasing temperature, q^* is already very close to q_f. Thus, in order to avoid arbitrariness, we choose to study the scaling behavior of q_f to show how q^* depends upon architectural parameters when a natural length scale emerges. The fact that this asymptotic value of q^* may correspond to a temperature wherein the WSL is no longer appropriate is not of concern because q_f is close to the value of q^* immediately after the regime where it varies sharply (where the WSL is appropriate).

Figure 3 shows the variation of the prefered wave vector q^* with M when N and P are fixed. We find three regimes. For small values of M, q_f decreases with increasing M. For large values of M, q_f is essentially independent of M. There is a transition region for the intermediate values of M. To understand the difference in the dependence of q_f on M we notice that when $M \gg N/P$, q_f is determined largely by the entropic cost of arranging the backbone segments to form periodic microdomains (because arranging branches is easier for larger values of M). Figure 4 clarifies this point. Here we plot q_f as a function of P in the region corresponding to a large value of M. From the dashed curves (where N and M are fixed), we find that $q_f \sim P^{1/2}$, or $q_f \sim (N/P)^{-1/2}$. This means the domain size is mainly determined by the average size of coils formed by backbone segments between two adjacent branch points. In contrast, when the value of M is small, M plays a more significant role in determining the domain size.

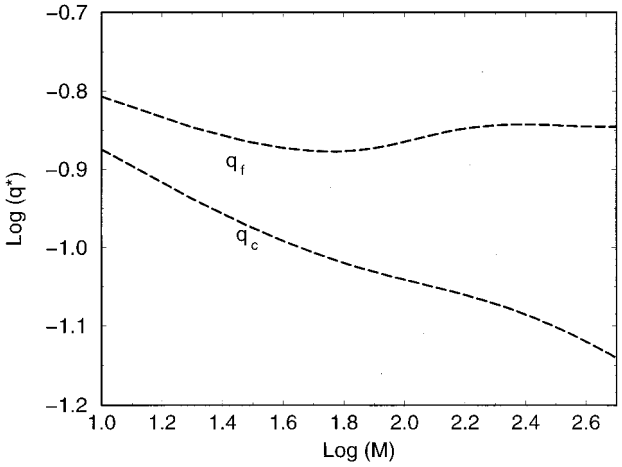

FIG. 3. Log–log plot of the dependence of the optimal wave vector for density fluctuations in the disordered phase, q_c, and the asymptotic value of the optimal wave vector in the LAM phase, q_f, on the branch length M. For both cases, $P=16$ and $N=2138$.

The relative importance of M and N/P in determining the prefered scale of ordering can also be understood as follows. In the one wave number approximation, the component with less volume fraction is always more significant in determining the domain size (in order to form a perfect, continuous periodic structure). For example, in DCPs, $q^* \sim (N_A N_B)^{-1/4}$. In the case of $N_A \gg N_B$ so that $N_A \approx N = \text{const}$, we have $q^* \sim N_B^{-1/4}$. Therefore, when $N/P \ll M$, N/P is dominant in determining the prefered scale of order-

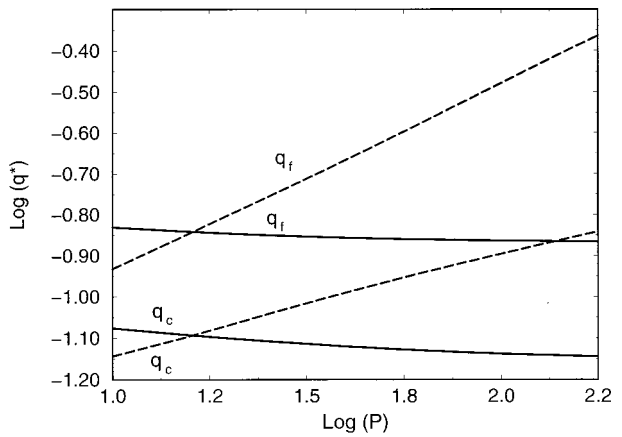

FIG. 4. Log–log plot of the dependence of the optimal wave vector for density fluctuations in the disordered phase, q_c, and the asymptotic value of the optimal wave vector in the LAM phase, q_f, on the number of branches P. The solid curves correspond to the constant values of $M=285$ and $N/P=2138/16$. The dashed curves correspond to the variation of holding $M=285$ and $N=2138$. The slope for q_f of the dashed curve is close to 1/2, and the slope for q_c of the dashed curve is close to 1/4. The magnitude of the slopes of both solid curves are smaller than 0.1.

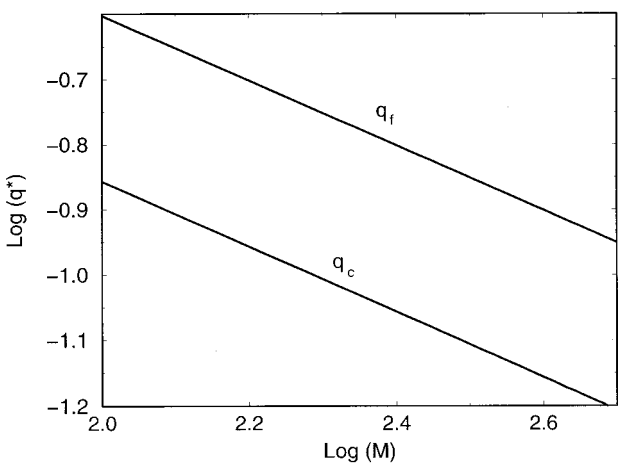

FIG. 5. Log–log plot of the dependence of the optimal wave vector for density fluctuations in the disordered phase, q_c, and the asymptotic value of the optimal wave vector in the LAM phase, q_f, on the branch length M. For both cases, $P=16$ and $N/M=2138/285$. The slopes are $-1/2$ for both curves.

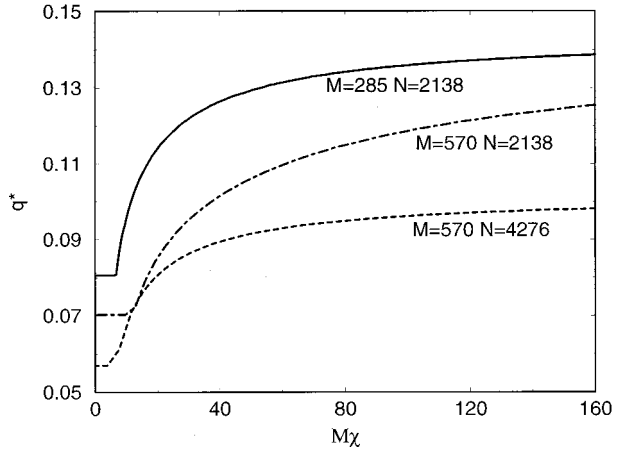

FIG. 6. The dependence of the optimal wave vector q^* on $M\chi$. For all three cases, the number of branches is $P=16$.

ing. When $M \ll N/P$, M plays a more important role in determining the natural length scale. However, N/P still plays a role. This is because making domains of one size out of backbone sections which exhibit quenched fluctuations leads to frustration not encounted in arranging the branches which all have the same length.

The solid curves in Fig. 4 correspond to the situation wherein N/P and M are fixed, but P and N are changing. Points on the abscissa therefore correspond to systems which at first glance appear to be architecturally similar (in a statistical sense). For a molten system of architecturally self-similar chains, we expect the domain size to scale with $X^{1/2}$, where X is the number of monomers per chain. In Fig. 4, the chain size is proportional to P, but we find that q_f essentially does not change upon such variations (the slope is ≈ 0.03; for q_c, the slope is ≈ 0.06). This means that this variation in architecture does not describe a self-similar transformation. In fact, as demonstrated in Fig. 5, for RGCs, the self-similar transformation is one where N/M and P are held fixed while changing M. As is evident, in this case, we find $q_f \sim M^{-1/2}$.

The width and the height of the windows wherein q^* changes rapidly, are also influenced by chain architecture. In Figs. 6 and 7 we show the change of window shape by showing the variation of q^* with $M\chi$ for different architectures. In Fig. 6, P is fixed at 16 for all three curves. By increasing M independently while holding the value of N constant (compare the solid curve to the dash-dotted curve), the width of the window increases much more than cases where M and N are increased proportionally (compare the solid curve to the dashed curve). In Fig. 7, M is fixed at 285 for all three curves. It is clear that by increasing P and holding N fixed, the width and the height of the window increase more than the case of increasing N and P proportionally.

IV. COMPARISON WITH EXPERIMENTS

Optical birefringence and SANS experiments were conducted on a 1 mm thick melt of the RGC held between optical flats. The RGC samples were prepared following procedures described in Ref. 14. Attention was focused on samples characterized by $N=2138$, $M=285$, and $P=16$. The reason for the choice of parameters in Fig. 1 should now be clear. The experiments were conducted over a temperature range of 110 °C and 180 °C (above the glass transition temperatures of PS and PB). The apparatus used for the optical experiments is described in Ref. 22. The temperature dependence of the measured optical signal is shown in Fig. 8. In previous studies of diblock copolymers,[22] it was shown that the order–disorder transition is announced by a discontinuous drop in the birefringence signal to less than 1 mV. The birefringence signal from the RGC melt is finite and comparable in magnitude to that obtained for ordered diblock copolymers[22] over the entire temperature range that was studied. This is indicative of an ordered phase; i.e., for these values of N, M, P, and density, the experiments were unable to access the MST. However, extrapolation of the birefringence data suggests that the MST occurs at $M\chi \sim O(10)$. This is consistent with the prediction in Fig. 1.

SANS experiments have also been conducted on molten RGCs at various temperatures.[14] A single scattering peak is

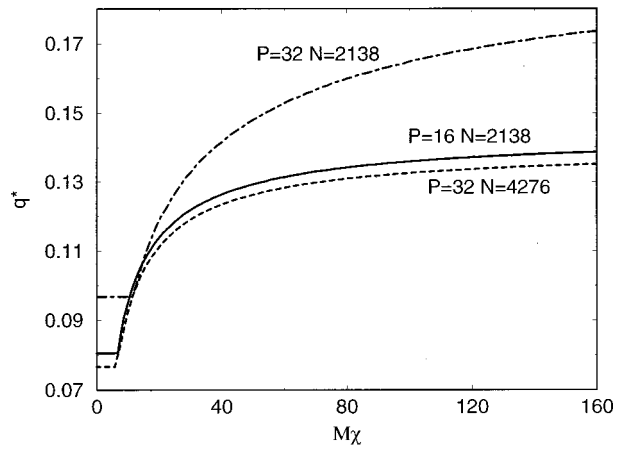

FIG. 7. The dependence of optimal wave vector q^* on $M\chi$. For the three cases, the branch length is $M=285$.

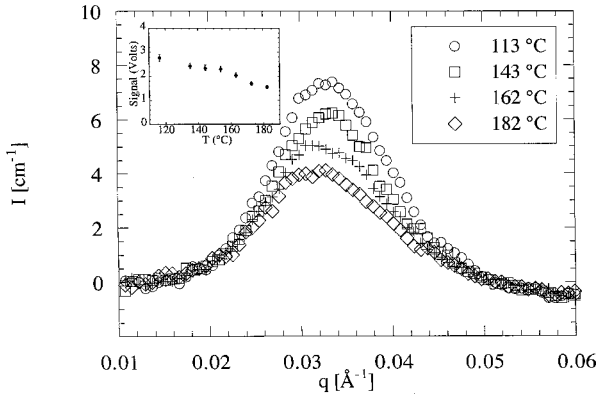

FIG. 8. Experimental data for a PS/PB RGC melt at selected temperatures in the ordered state. Main figure: SANS data; inset: optical birefringence.

evident at all temperatures, and the coherent scattering intensity goes to zero (within experimental uncertainty) in both high and low q limits. These features, coupled with finite birefringence signals, are classic signatures of microphase ordering in weakly ordered systems (e.g., Ref. 22). However, the widths of the scattering peaks in Fig. 8 are considerably larger than those seen for ordered diblock copolymers.[1] This is clearly the effect of randomness in branch point location.

The order parameter in our theory is characterized by two parameters, q^* and the scattering intensity at the peak ($I^* \sim |D|^2$). Figure 9 compares the experimentally determined I^* with theory. We assume that χ has the familiar temperature dependence $\chi = A + B/T$ and adjust the values of A and B to obtain the best fit to the experimental data. We find that A is vanishingly small (~ 0.003), and $B = 20$ obtains the best fit shown in Fig. 9. This value of B is in agreement with that reported[23] for a PS/PB diblock copolymer ($B = 19$). This is reassuring as the value of B is largely determined by the intersegment interactions, and thus should be roughly the same for a given chemistry. These values of A and B allow us to relate the temperatures at which the experiments were conducted to the χ parameters used in the theoretical calculations. According to Fig. 1, the values of $M\chi$ corresponding to the measured temperature place the experimental data in a region close to the crossover from

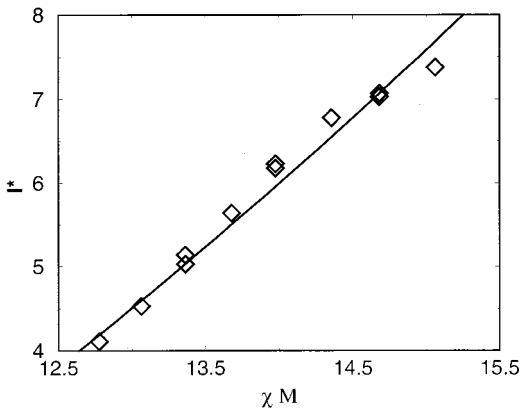

FIG. 9. Peak scattering intensity in SANS experiments as a function of $M\chi$. ○ symbols are measured values, and the curve represents the theoretical fit.

strongly temperature dependent to essentially temperature independent values of q^*. In this window, our theory indicates (using $b = 5.02$ Å for PS)[23] that q^* should lie between 0.025 to 0.026 Å^{-1}. For reference, we also note that the asymptotic value of q^* deep in the ordered region (Fig. 1) is 0.031 Å^{-1}. Differences of less than 0.001 Å^{-1} are not resolved in the experiments. Hence, even though there is a systematic decrease in q^* with temperature (see Fig. 8), we conservatively conclude that, within experimental uncertainties, q^* is independent of temperature in the measured range and equals 0.032 ± 0.001 Å^{-1}. The agreement between theory and experiment is reasonable considering the experimental uncertainties in χ, M, N, and P.

V. CONCLUSIONS

In this paper we derive a Landau free energy functional for RGC melts. In this system, competing interactions and chain connectivity are further frustrated by the quenched randomness embodied in the location of the branch points. We use the free energy functional to investigate microphase ordering in molten RGCs. In the weak segregation limit, we find that the optimal wave vector q^* characterizing domain size in the lamellar phase sharply increases immediately below the MST, and then acquires an asymptotic value at lower temperatures. This result is very different from that of either DCPs (q^* decreases around the MST) or LRCs (q^* increases indefinitely). Physically, this unusual behavior is explained in terms of the length scales of the system. The key player here is the random distribution of branch points. It provides the freedom to acquire continuously smaller domain spacing to compensate for the increasing energetic driving force for microphase separation upon decreasing temperature. However, ultimately a natural length scale emerges (either N/P or M) which determines the asymptotic value. Our analytical results are compared with the SANS data and optical birefringence data[14] and we find good agreement. The variation of domain size with temperature (and its dependence on architecture) suggests a new way of controlling and changing the size of micropatterned domains by exploiting quenched disorder embodied in the sequence of RGCs.

It is appropriate to close by pointing out the main limitations of our theory. This theory is based on a Gaussian chain approximation, so it is only valid for $N \gg 1$ and $M \gg 1$. In deriving the cubic and quartic terms in the free energy functional, we treat P as a large value. This simplifies the calculation but causes trouble when extrapolating the theory to discuss microphase ordering for small values of P. We use the one wave number approximation. Thus we ignore chain stretching in this theory. We realize that at lower temperatures chain stretching plays an important role in determining phase spacing, and a theory accounting for chain stretching would be interesting to study. Nevertheless, because of the dominance of the quenched randomness in this system, we believe that the tendency for q^* to rapidly increase upon decreasing temperature is very strong for RGCs immediately below the MST.

ACKNOWLEDGMENTS

Financial support is provided by U.S.D.O.E. (Basic Energy Sciences). The authors are very grateful to Professor E. I. Shakhnovich for numerous fruitful discussions and collaborations on the physics of RGCs.

APPENDIX A

To obtain the average entropy $\langle S\rangle$ as a functional of coarse-grained density fields, we employ a mean field approach[16] and carry out the quenched average using the replica method. First, we introduce the identity

$$
\begin{aligned}
1=&\Pi_{\alpha=1}^{\sigma}\int D\rho_A^{\alpha}(\mathbf{r})D\rho_B^{\alpha}(\mathbf{r})\,\delta\left[\rho_A^{\alpha}(\mathbf{r})-\int dn\,\delta[\mathbf{r}-\mathbf{r}^{\alpha}(n)]\right]\\
&\times\delta\left[\rho_B^{\alpha}(\mathbf{r})-\sum_{j=1}^{P}\int ds\,\delta[\mathbf{r}-\mathbf{r}_j^{\alpha}(s)]\right]\\
=&\Pi_{\alpha=1}^{\sigma}\int D\rho_A^{\alpha}(\mathbf{r})D\rho_B^{\alpha}(\mathbf{r})D\gamma_A^{\alpha}(\mathbf{r})D\gamma_B^{\alpha}(\mathbf{r})\\
&\times\exp\left\{i\int d\mathbf{r}[\gamma_A^{\alpha}(\mathbf{r})\rho_A^{\alpha}(\mathbf{r})+\gamma_B^{\alpha}(\mathbf{r})\rho_B^{\alpha}(\mathbf{r})]\right.\\
&\left.-i\left[\int dn\,\gamma_A^{\alpha}(\mathbf{r}^{\alpha}(n))+\sum_{j=1}^{P}\int ds\,\gamma_B^{\alpha}(\mathbf{r}_j^{\alpha}(s))\right]\right\}. \qquad \text{(A1)}
\end{aligned}
$$

Here $\gamma_A(\mathbf{r})$ and $\gamma_B(\mathbf{r})$ are fields conjugated to $\rho_A(\mathbf{r})$ and $\rho_B(\mathbf{r})$, respectively. Substituting the above identity into Eq. (6) obtains:

$$
\begin{aligned}
\langle R^{\sigma}\rangle=&\Pi_{\alpha=1}^{\sigma}\int D\rho_A^{\alpha}(\mathbf{r})D\rho_B^{\alpha}(\mathbf{r})D\gamma_A^{\alpha}(\mathbf{r})D\gamma_B^{\alpha}(\mathbf{r})\\
&\times\exp\left\{i\int d\mathbf{r}[\gamma_A^{\alpha}(\mathbf{r})\rho_A^{\alpha}(\mathbf{r})+\gamma_B^{\alpha}(\mathbf{r})\rho_B^{\alpha}(\mathbf{r})]\right\}\\
&\times\left\langle\Pi_{j=1}^{P}\int D\mathbf{r}^{\alpha}(n)D\mathbf{r}_j^{\alpha}(s)P[\mathbf{r}^{\alpha}(n)]P[\mathbf{r}_j^{\alpha}(s)]\right.\\
&\left.\times\delta[\mathbf{r}_j^{\alpha}(0)-\mathbf{r}^{\alpha}(\tau_j)]\right\rangle, \qquad \text{(A2)}
\end{aligned}
$$

where

$$
P[\mathbf{r}^{\alpha}(n)]=P_0[\mathbf{r}^{\alpha}(n)]\exp\left\{-i\int dn\,\gamma_A^{\alpha}(\mathbf{r}^{\alpha}(n))\right\},
$$

$$
P[\mathbf{r}_j^{\alpha}(s)]=P_0[\mathbf{r}_j^{\alpha}(s)]\exp\left\{-i\int ds\,\gamma_B^{\alpha}(\mathbf{r}_j^{\alpha}(s))\right\}. \qquad \text{(A3)}
$$

The part which has to be averaged over the quenched distribution of branch points is:

$$
\begin{aligned}
\langle Q^{\sigma}\rangle=&\left\langle\Pi_{\alpha=1}^{\sigma}\Pi_{j=1}^{p}\int D\mathbf{r}^{\alpha}(n)D\mathbf{r}_j^{\alpha}(s)\right.\\
&\left.\times P[\mathbf{r}^{\alpha}(n)]P[\mathbf{r}_j^{\alpha}(s)]\delta[\mathbf{r}_j^{\alpha}(0)-\mathbf{r}^{\alpha}(\tau_j)]\right\rangle\\
=&\left\langle\left\{\Pi_{j=1}^{p}\int D\mathbf{r}(n)D\mathbf{r}_j(s)\right.\right.\\
&\left.\left.\times P[\mathbf{r}(n)]P[\mathbf{r}_j(s)]\delta[\mathbf{r}_j(0)-\mathbf{r}(\tau_j)]\right\}^{\sigma}\right\rangle. \qquad \text{(A4)}
\end{aligned}
$$

We now use a perturbation method and expand $\langle Q\rangle$ in cumulants by powers of the conjugated fields γ_A and γ_B:

$$
Q=Q_0+Q_1+Q_2+Q_3+Q_4+\cdots, \qquad \text{(A5)}
$$

where Q_n is to the nth power of the conjugated fields. Q_0 is the unperturbed case ($\gamma_A=\gamma_B=0$), and it is easy to obtain $Q_0=V$. The linear term Q_1 contributes a constant to the free energy formula. The first nontrivial term is Q_2. After transforming the fields and propagators into Fourier space, we obtain

$$
Q_2=-\frac{1}{2}\int d\mathbf{q}\boldsymbol{\gamma}^T(q)M(\mathbf{q})\boldsymbol{\gamma}(q), \qquad \text{(A6)}
$$

where $\boldsymbol{\gamma}^T=(\gamma_A,\gamma_B)$ and M is a 2×2 matrix:

$$
\begin{aligned}
M_{11}(q)&=\frac{2}{x^2}[Nx+\exp(-Nx)-1]=N^2g_2(Nx),\\
M_{22}(q)&=PM^2g_2(Mx)+P(P-1)M^2g_1(Mx)^2g_2(Nx),\\
M_{12}(q)&=M_{21}(q)=NPMg_1(Mx)g_2(Nx),
\end{aligned} \qquad \text{(A7)}
$$

where $x=q^2b^2/6$. Here we define $g_1(y)=[1-\exp(-y)]/y$ and $g_2(y)=(2/y^2)[y+\exp(-y)-1]$. $g_2(y)$ is the so-called Debye function.

Similarly, we derive the expressions for Q_3 and Q_4 as functionals of the conjugated fields. In Appendix B we show how to get a typical term in Q_4 by exploiting a graphical method. Here we only present the results of this calculation:

$$
\begin{aligned}
\langle Q\rangle=&V-\frac{1}{2}\int d\mathbf{q}\boldsymbol{\gamma}^T(\mathbf{q})M(\mathbf{q})\boldsymbol{\gamma}(\mathbf{q})+\frac{i}{6}\int d\mathbf{q}_1\,d\mathbf{q}_2[\Gamma_{30}(\mathbf{q}_1,\mathbf{q}_2)\gamma_A(\mathbf{q}_1)\gamma_A(\mathbf{q}_2)\gamma_A(-\mathbf{q}_1-\mathbf{q}_2)+\Gamma_{31}(\mathbf{q}_1,\mathbf{q}_2)\\
&\times\gamma_A(\mathbf{q}_1)\gamma_A(\mathbf{q}_2)\gamma_B(-\mathbf{q}_1-\mathbf{q}_2)+\Gamma_{32}(\mathbf{q}_1,\mathbf{q}_2)\gamma_A(\mathbf{q}_1)\gamma_B(\mathbf{q}_2)\gamma_B(-\mathbf{q}_1-\mathbf{q}_2)+\Gamma_{33}(\mathbf{q}_1,\mathbf{q}_2)\gamma_B(\mathbf{q}_1)\gamma_B(\mathbf{q}_2)\\
&\times\gamma_B(-\mathbf{q}_1-\mathbf{q}_2)]+\frac{1}{24}\int d\mathbf{q}_1\,d\mathbf{q}_2\,d\mathbf{q}_3[\Gamma_{40}(\mathbf{q}_1,\mathbf{q}_2,\mathbf{q}_3)\gamma_A(\mathbf{q}_1)\gamma_A(\mathbf{q}_2)\gamma_A(\mathbf{q}_3)\gamma_A(-\mathbf{q}_1-\mathbf{q}_2-\mathbf{q}_3)+\Gamma_{41}(\mathbf{q}_1,\mathbf{q}_2,\mathbf{q}_3)\gamma_A(\mathbf{q}_1)\\
&\times\gamma_A(\mathbf{q}_2)\gamma_A(\mathbf{q}_3)\gamma_B(-\mathbf{q}_1-\mathbf{q}_2-\mathbf{q}_3)+\Gamma_{42}(\mathbf{q}_1,\mathbf{q}_2,\mathbf{q}_3)\gamma_A(\mathbf{q}_1)\gamma_A(\mathbf{q}_2)\gamma_B(\mathbf{q}_3)\gamma_B(-\mathbf{q}_1-\mathbf{q}_2-\mathbf{q}_3)+\Gamma_{43}(\mathbf{q}_1,\mathbf{q}_2,\mathbf{q}_3)\gamma_A(\mathbf{q}_1)\\
&\times\gamma_B(\mathbf{q}_2)\gamma_B(\mathbf{q}_3)\gamma_B(-\mathbf{q}_1-\mathbf{q}_2-\mathbf{q}_3)+\Gamma_{44}(\mathbf{q}_1,\mathbf{q}_2,\mathbf{q}_3)\gamma_B(\mathbf{q}_1)\gamma_B(\mathbf{q}_2)\gamma_B(\mathbf{q}_3)\gamma_B(-\mathbf{q}_1-\mathbf{q}_2-\mathbf{q}_3)], \qquad \text{(A8)}
\end{aligned}
$$

where the functions $\Gamma_{3i}(\mathbf{q}_1,\mathbf{q}_2)$ are

$$(2\pi)^{3/2}\Gamma_{30}=6N^3h_2(Nx_1,Nx_2),$$

$$(2\pi)^{3/2}\Gamma_{31}=6(PM)N^2g_1(Mx_2[2h_2)(Nx_1,Nx_2)+h_2(Nx_1,Nx_3)],$$

$$(2\pi)^{3/2}\Gamma_{32}=3\Bigg\{PM^2Ng_2(Nx_1)H_2(Mx_1-Mx_2,Mx_2)+4(PM)^2Ng_1(Mx_2)g_1(Mx_3)h_2(Nx_1,Nx_2)$$
$$+(PM)^2g_1(Mx_2)g_1(Mx_3)\frac{g_2(Nx_2)-g_2(Nx_3)}{x_3-x_2}\Bigg\},$$

$$(2\pi)^{3/2}\Gamma_{33}=6PM^3h_2(Mx_1,Mx_2)+6\{P^2M^3g_2(Nx_2)g_1(Mx_2)H_2(Mx_2-Mx_1-Mx_1)$$
$$+(PM)^3g_1(Mx_1)g_1(Mx_2)g_1(Mx_3)h_2(Nx_1,Nx_3)\}, \tag{A9}$$

where $x_i=q_i^2b^2/6$ for $i=1$, 2 and $x_3=(\mathbf{q}_1+\mathbf{q}_2)^2b^2/6$. Functions $\Gamma_{4i}(\mathbf{q}_1,\mathbf{q}_2,\mathbf{q}_3)$ are:

$$(2\pi)^3\Gamma_{40}=24N^4h_3(Nx_1,Nx_7,Nx_4),$$

$$(2\pi)^3\Gamma_{41}=96PMN^3g_1(Mx_4)h_3(Nx_1,Nx_7,Nx_4),$$

$$(2\pi)^3\Gamma_{42}=12\Bigg\{2PM^2N^2H_2(-Mx_4,Mx_4+Mx_7)[2h_2(Nx_1,Nx_7)+h_2(Nx_1,Nx_2)]$$
$$+4(PMN)^2g_1(Mx_3)g_1(Mx_4)h_3(Nx_1,Nx_7,Nx_3)+\frac{(PM)^2}{x_4-x_6}g_1(Mx_3)g_1(Mx_4)\Bigg[\frac{g_2(Nx_3)-g_2(Nx_6)}{x_6-x_3}$$
$$-\frac{g_2(Nx_3)-g_2(Nx_4)}{x_4-x_3}\Bigg]+\frac{4(PMN)^2}{N(x_6-x_4)}g_1(Mx_3)g_1(Mx_4)[h_2(Nx_1,Nx_4)-h_2(Nx_1,Nx_6)]$$
$$+2(PMN)^2g_1(Mx_3)g_1(Mx_4)h_3(Nx_1,Nx_6,Nx_2)\Bigg\},$$

$$(2\pi)^3\Gamma_{43}=8\Bigg\{3NPM^3g_2(Nx_1)H_3(Mx_1-Mx_7,Mx_7-Mx_4,Mx_4)+\frac{12P^2M^3}{x_1}h_2(Nx_1,Nx_2)H_2(-Mx_4,Mx_4+Mx_7)$$
$$\times g_1(Mx_2)+3P^2M^3g_1(Mx_4)\frac{g_2(Nx_5)-g_2(Nx_4)}{x_4-x_5}H_2(-Mx_2,Mx_2+Mx_5)$$
$$+6\frac{(PM)^3}{x_1}g_1(Mx_2)g_1(Mx_3)g_1(Mx_4)[h_2(Nx_7,Nx_3)-H_3(Nx_1-Nx_7,Nx_7-Nx_3,Nx_3)]$$
$$+6(PM)^3g_1(Mx_2)g_1(Mx_3)g_1(Mx_4)\frac{h_2(Nx_2,Nx_4)-h_2(Nx_7,Nx_4)}{x_7-x_2}\Bigg\},$$

$$(2\pi)^3\Gamma_{44}=24PM^4h_3(Mx_1,Mx_7,Mx_4)+24P^2M^4g_1(Mx_1)H_3(Mx_1-Mx_7,Mx_7-Mx_4,Mx_4)g_2(Nx_1)$$
$$+12P^2M^4g_2(Nx_7)H_2(-Mx_1,Mx_1+Mx_7)H_2(-Mx_4,Mx_4+Mx_7)$$
$$+72P^3M^4g_1(Mx_1)g_1(Mx_2)h_2(Nx_1,Nx_7)H_2(-Mx_4,Mx_4+Mx_7)$$
$$+24(PM)^4g_1(Mx_1)g_1(Mx_2)g_1(Mx_3)g_1(Mx_4)h_3(Nx_1,Nx_7,Nx_4), \tag{A10}$$

where $x_i=q_i^2b^2/6$ for $i=1,2,3$, and $x_4=(\mathbf{q}_1+\mathbf{q}_2+\mathbf{q}_3)^2b^2/6$, $x_5=(\mathbf{q}_2+\mathbf{q}_3)^2b^2/6$, $x_6=(\mathbf{q}_1+\mathbf{q}_3)^2b^2/6$ and $x_7=(\mathbf{q}_1+\mathbf{q}_2)^2b^2/6$. In these expressions, we have defined the following functions:

$$h_1(y_1)=\int_0^1 dn_2\int_0^{n_2}dn_1\exp[-n_2-n_1)y_1]$$
$$=\frac{1-g_1(y_1)}{y_1}=\frac{g_2(y_1)}{2},$$

$$h_2(y_1,y_2)=\int_0^1 dn_3\int_0^{n_3}dn_2\int_0^{n_2}dn_1$$
$$\times\exp[-(n_2-n_1)y_1-(n3-n_2)y_2]$$
$$=\frac{1}{y_1}\Bigg[h_1(y_2)-\frac{g_1(y_2)-g_1(y_1)}{y_1-y_2}\Bigg],$$

$$h_3(y_1,y_2,y_3)=\int_0^1 dn_4\int_0^{n_4} dn_3\int_0^{n_3} dn_2\int_0^{n_2} dn_1 \times\exp[-(n_2-n_1)(y_1-(n3-n_2)y_2 -(n_4-n_3)y_3] =\frac{1}{y_1}\left\{h_2(y_2,y_3)-\frac{1}{y_1-y_2} \times\left[\frac{g_1(y_2)-g_1(y_3)}{y_3-y_2}-\frac{g_1(y_1)-g_1(y_3)}{y_3-y_1}\right],\right.$$

$$H_2(y_1,y_2)=\int_0^1 dn_2\int_0^{n_2} dn_1\exp[-n_1y_1-n_2y_2] =\frac{1}{y_1}[g_1(y_2)-g_1(y_1+y_2)],$$

$$H_3(y_1,y_2,y_3)=\int_0^1 dn_3\int_0^{n_3} dn_2\int_0^{n_2} dn_1 \times\exp[-n_1y_1-n_2y_2-n_3y_3] =\frac{1}{y_1}[H_2(y_2,y_3)-H_2(y_1+y_2,y_3)].$$

(A11)

From this, we obtain the expression of $\langle Q^\sigma\rangle$:

$$\left\langle\left(\frac{Q}{V}\right)^\sigma\right\rangle=1+\frac{1}{V}\sum_{\alpha=1}^{\sigma}\left\{-\frac{1}{2}\int d\mathbf{q}_\alpha\boldsymbol{\gamma}^T(\mathbf{q}^\alpha)M(\mathbf{q}^\alpha)\boldsymbol{\gamma}(\mathbf{q}^\alpha)+\frac{i}{6}\int d\mathbf{q}_1^\alpha d\mathbf{q}_2^\alpha[\Gamma_{30}(\mathbf{q}_1^\alpha,\mathbf{q}_2^\alpha)\gamma_A(\mathbf{q}_1^\alpha)\gamma_A(\mathbf{q}_2^\alpha)\gamma_A-(\mathbf{q}_1^\alpha-q_2^\alpha)\right.$$
$$+\Gamma_{31}(\mathbf{q}_1^\alpha,\mathbf{q}_2^\alpha)\gamma_A(\mathbf{q}_1^{\alpha a})\gamma_A(\mathbf{q}_2^\alpha)\gamma_B-(\mathbf{q}_1^\alpha-\mathbf{q}_2^\alpha)+\Gamma_{32}(\mathbf{q}_1^\alpha,\mathbf{q}_2^\alpha)\gamma_A(\mathbf{q}_1^\alpha)\gamma_B(\mathbf{q}_2^\alpha)\gamma_B(-\mathbf{q}_1^\alpha-\mathbf{q}_2^\alpha)$$
$$\left.+\Gamma_{33}(\mathbf{q}_1^\alpha,\mathbf{q}_2^\alpha)\gamma_B(\mathbf{q}_1^\alpha)\gamma_B(\mathbf{q}_2^\alpha)\gamma_B(-\mathbf{q}_1^\alpha-\mathbf{q}_2^\alpha)]+\frac{1}{24}\int d\mathbf{q}_1^\alpha d\mathbf{q}_2^\alpha d\mathbf{q}_3^\alpha[\Gamma_{40}(\mathbf{q}_1^\alpha,\mathbf{q}_2^\alpha,\mathbf{q}_3^\alpha)\gamma_A(\mathbf{q}_1^\alpha)\gamma_A(\mathbf{q}_2^\alpha)\gamma_A(\mathbf{q}_3^\alpha)\right.$$
$$\times\gamma_A(-\mathbf{q}_1^\alpha-\mathbf{q}_2^\alpha-\mathbf{q}_3^\alpha)+\Gamma_{41}(\mathbf{q}_1^\alpha,\mathbf{q}_2^\alpha,\mathbf{q}_3^{ga})\gamma_A(\mathbf{q}_1^\alpha)\gamma_A(\mathbf{q}_2^\alpha)\gamma_A(\mathbf{q}_3^\alpha)\gamma_B(-\mathbf{q}_1^\alpha-\mathbf{q}_2^\alpha-\mathbf{q}_3^\alpha)$$
$$+\Gamma_{42}(\mathbf{q}_1^\alpha,\mathbf{q}_2^\alpha,\mathbf{q}_3^{ga})\gamma_A(\mathbf{q}_1^\alpha)\gamma_A(\mathbf{q}_2^\alpha)$$
$$\times\gamma_B(\mathbf{q}_3^\alpha)\gamma_B(-\mathbf{q}_1^\alpha-\mathbf{q}_2^\alpha-\mathbf{q}_3^\alpha)+\Gamma_{43}(\mathbf{q}_1^\alpha,\mathbf{q}_2^\alpha,\mathbf{q}_3^{ga})\gamma_A(\mathbf{q}_1^\alpha)\gamma_B(\mathbf{q}_2^\alpha)\gamma_B(\mathbf{q}_3^\alpha)\gamma_B(-\mathbf{q}_1^\alpha-\mathbf{q}_2^\alpha-\mathbf{q}_3^\alpha)$$
$$+\Gamma_{44}(\mathbf{q}_1^\alpha,\mathbf{q}_2^\alpha,\mathbf{q}_3^{ga})\gamma_B(\mathbf{q}_1^\alpha)$$
$$\left.\left.\times\gamma_B(\mathbf{q}_2^\alpha)\gamma_B(\mathbf{q}_3^\alpha)\gamma_B(-\mathbf{q}_1^\alpha-\mathbf{q}_2^\alpha-\mathbf{q}_3^\alpha)]\right\}+\frac{1}{4}\sum_{\alpha\neq\beta}^{\sigma}\int d\mathbf{q}^\alpha d\mathbf{q}^\beta\langle\boldsymbol{\gamma}^\alpha(\mathbf{q}^\alpha)M_0(\mathbf{q}^\alpha)\boldsymbol{\gamma}(\mathbf{q}^\alpha)\boldsymbol{\gamma}^T(\mathbf{q}^\beta)M_0(\mathbf{q}^\beta)\boldsymbol{\gamma}(\mathbf{q}^\beta)\rangle,\right.$$

(A12)

where the matrix M_0 is:

$$(M_0)_{11}(q)=\sum_{j=1}^{P+1}\frac{2}{x^2}\{(\tau_j-\tau_{j-1})x+\exp[-(\tau_j-\tau_{j-1})x]-1\} +2\sum_{i<j}^{P+1}\frac{\exp(\tau_ix)-\exp(\tau_{i-1}x)}{x} \times\frac{\exp(-\tau_{j-1}x)-\exp(-\tau_jx)}{x},$$

$$(M_0)_{22}(q)=PM^2g(Mx)+2\left[\frac{1-\exp(-Mx)}{x}\right]^2 \times\sum_{i<j}^{P}\exp[-x(\tau_j-\tau_i)],$$

$$(M_0)_{12}(q)=(M_0)_{21}(q) =\frac{1-\exp(-Mx)}{x}\sum_{i=1}^{P+1}\sum_{j=1}^{P} \times\left|\frac{\exp(-x|\tau_j-\tau_i|)-\exp(-x|\tau_j-\tau_{i-1}|)}{x}\right|,$$

(A13)

and it satisfies $\langle M_0\rangle=M$. Now we have

$$\langle R^\sigma\rangle[\rho_A,\rho_B,\gamma_A,\gamma_B] =\Pi_{\alpha=1}^{\alpha}\int D\rho_A^\alpha(\mathbf{q})D\rho_B^\alpha(\mathbf{q})D\gamma_A^\alpha(\mathbf{q})D\gamma_B^\alpha(\mathbf{q})\exp \times\left\{i\int d\mathbf{q}[\gamma_A^\alpha(\mathbf{q})\rho_A^\alpha(-\mathbf{q})+\gamma_B^\alpha(\mathbf{q})\rho_B^\alpha(-\mathbf{q})]\right\}\langle Q^\sigma\rangle,$$

(A14)

where $\langle Q^\sigma\rangle$ is presented in Eq. (A12).

As in the case for systems with ordered architectures (e.g., DCPs and triblock copolymers), it is impossible to obtain an analytic formula for the free energy functional by

explicitly performing the functional integrations in Eq. (A14). Thus we evaluate these functional integrals using the saddle point approximation. This yields:

$$\langle R^{\sigma}\rangle[\rho_A,\rho_B,\gamma_A,\gamma_B]\approx\langle R^{\sigma}\rangle_{s.p.}[\rho_A,\rho_B,\gamma_{As.p.},\gamma_{Bs.p.}], \tag{A15}$$

where $\gamma^{\alpha}_{As.p.}(\mathbf{q})$ and $\gamma^{\alpha}_{Bs.p.}(\mathbf{q})$ satisfy

$$\frac{\delta \ln\langle R^{\sigma}\rangle[\rho_A,\rho_B,\gamma_A,\gamma_B]}{\delta\gamma^{\alpha}_A(-\mathbf{q})}=0,$$
$$\frac{\delta \ln\langle R^{\sigma}\rangle[\rho_A,\rho_B,\gamma_A,\gamma_B]}{\delta\gamma^{\alpha}_B(-\mathbf{q})}=0. \tag{A16}$$

Solving the above equations by iteration, we obtain $\langle S[\rho_A,\rho_B]\rangle=\lim_{k\to 0}[\langle R^{\sigma}\rangle_{s.p.}[\rho_A,\rho_B]-1]/k$ as a functional of ρ_A and ρ_B:

$$\begin{aligned}\langle S[\rho_A,\rho_B]\rangle=&-\frac{V}{2}\int d\mathbf{q}\boldsymbol{\rho}^T W\boldsymbol{\rho}+\frac{i}{6V}\int d\mathbf{q}_1\,d\mathbf{q}_2[\Gamma_{30}(\mathbf{q}_1,\mathbf{q}_2)\gamma_{1A}(\mathbf{q}_1)\gamma_{1A}(\mathbf{q}_2)\gamma_{1A}(-\mathbf{q}_1-\mathbf{q}_2)\\
&+\Gamma_{31}(\mathbf{q}_1,\mathbf{q}_2)\gamma_{1A}(\mathbf{q}_1)\gamma_{1A}(\mathbf{q}_2)\gamma_{1B}(-\mathbf{q}_1-\mathbf{q}_2)+\Gamma_{32}(\mathbf{q}_1,\mathbf{q}_2)\gamma_{1A}(\mathbf{q}_1)\gamma_{1B}(\mathbf{q}_2)\gamma_{1B}(-\mathbf{q}_1-\mathbf{q}_2)\\
&+\Gamma_{33}(\mathbf{q}_1,\mathbf{q}_2)\gamma_{1B}(\mathbf{q}_1)\gamma_{1B}(\mathbf{q}_2)\gamma_{1B}(-\mathbf{q}_1-\mathbf{q}_2)]+\frac{1}{24V}\int d\mathbf{q}_1\,d\mathbf{q}_2\,d\mathbf{q}_3[\Gamma'_{40}(\mathbf{q}_1,\mathbf{q}_2,\mathbf{q}_3)\gamma_{1A}(\mathbf{q}_1)\gamma_{1A}(\mathbf{q}_2)\\
&\times\gamma_{1A}(\mathbf{q}_3)\gamma_{1A}(-\mathbf{q}_1-\mathbf{q}_2-\mathbf{q}_3)+\Gamma'_{41}(\mathbf{q}_1,\mathbf{q}_2,\mathbf{q}_3)\gamma_{1A}(\mathbf{q}_1)\gamma_{1A}(\mathbf{q}_2)\gamma_{1A}(\mathbf{q}_3)\gamma_{1B}(-\mathbf{q}_1-\mathbf{q}_2-\mathbf{q}_3)+\Gamma'_{42}(\mathbf{q}_1,\mathbf{q}_2,\mathbf{q}_3)\\
&\times\gamma_{1A}(\mathbf{q}_1)\gamma_{1A}(\mathbf{q}_2)\gamma_{1B}(\mathbf{q}_3)\gamma_{1B}(-\mathbf{q}_1-\mathbf{q}_2-\mathbf{q}_3)+\Gamma'_{43}(\mathbf{q}_1,\mathbf{q}_2,\mathbf{q}_3)\gamma_{1A}(\mathbf{q}_1)\gamma_{1B}(\mathbf{q}_2)\gamma_{1B}(\mathbf{q}_3)\gamma_{1B}(-\mathbf{q}_1-\mathbf{q}_2-\mathbf{q}_3)\\
&+\Gamma'_{44}(\mathbf{q}_1,\mathbf{q}_2,\mathbf{q}_3)\gamma_{1B}(\mathbf{q}_1)\gamma_{1B}(\mathbf{q}_2)\gamma_{1B}(\mathbf{q}_3)\gamma_{1B}(-\mathbf{q}_1-\mathbf{q}_2-\mathbf{q}_3)]-\frac{1}{8V^2}\int d\mathbf{q}_1\,d\mathbf{q}_2\{\langle\boldsymbol{\gamma}_1^T(\mathbf{q}_1)M_0(\mathbf{q}_1)\boldsymbol{\gamma}_1(\mathbf{q}_1)\\
&\times\boldsymbol{\gamma}_1^T(\mathbf{q}_2)M_0(\mathbf{q}_2)\boldsymbol{\gamma}_1(\mathbf{q}_2)\rangle-[\boldsymbol{\gamma}_1^T(\mathbf{q}_1)M(\mathbf{q}_1)\boldsymbol{\gamma}_1(\mathbf{q}_1)][\gamma_1^T(\mathbf{q}_2)M(\mathbf{q}_2)\boldsymbol{\gamma}_1(\mathbf{q}_2)]\},\end{aligned} \tag{A17}$$

where the matrix W is the inverse of M and $\gamma_{1A}=iV(W_{11}\rho_A+W_{12}\rho_B)$, $\gamma_{1B}=iV(W_{12}\rho_A+W_{22}\rho_B)$, and $\boldsymbol{\gamma}_1^T=(\gamma_{1A},\gamma_{1B})$. The modified quartic coefficients are:

$$\begin{aligned}\Gamma'_{40}(\mathbf{q}_1,\mathbf{q}_2,\mathbf{q}_3)=&\Gamma_{40}(\mathbf{q}_1,\mathbf{q}_2,\mathbf{q}_3)-\tfrac{1}{3}\{[\Gamma_{30}(\mathbf{q}_1+\mathbf{q}_2,\mathbf{q}_3)+\Gamma_{30}(\mathbf{q}_3,\mathbf{q}_1+\mathbf{q}_2)+\Gamma_{30}(\mathbf{q}_3,\mathbf{q}_4)]W_{11}(\mathbf{q}_1+\mathbf{q}_2)[\Gamma_{30}(-\mathbf{q}_1-\mathbf{q}_2,\mathbf{q}_1)\\
&+\Gamma_{30}(\mathbf{q}_1,-\mathbf{q}_1-\mathbf{q}_2)+\Gamma_{30}(\mathbf{q}_1,\mathbf{q}_2)]+2[\Gamma_{30}(\mathbf{q}_1+\mathbf{q}_2,\mathbf{q}_3)+\Gamma_{30}(\mathbf{q}_3,\mathbf{q}_1+\mathbf{q}_2)+\Gamma_{30}(\mathbf{q}_3,\mathbf{q}_4)]W_{12}(\mathbf{q}_1+\mathbf{q}_2)\\
&\times\Gamma_{31}(\mathbf{q}_1,\mathbf{q}_2)+\Gamma_{31}(\mathbf{q}_1,\mathbf{q}_2)M_{22}(\mathbf{q}_1+\mathbf{q}_2)\Gamma_{31}(\mathbf{q}_3,\mathbf{q}_4)\},\end{aligned}$$

$$\begin{aligned}\Gamma'_{41}(\mathbf{q}_1,\mathbf{q}_2,\mathbf{q}_3)=&\Gamma_{41}(\mathbf{q}_1,\mathbf{q}_2,\mathbf{q}_3)-\tfrac{1}{3}\{2[\Gamma_{30}(-\mathbf{q}_1-\mathbf{q}_2,\mathbf{q}_1)+\Gamma_{30}(\mathbf{q}_1,-\mathbf{q}_1-\mathbf{q}_2)+\Gamma_{30}(\mathbf{q}_1,\mathbf{q}_2)]W_{11}(\mathbf{q}_1+\mathbf{q}_2)[\Gamma_{31}(\mathbf{q}_1+\mathbf{q}_2,\mathbf{q}_3)\\
&+\Gamma_{31}(\mathbf{q}_3,\mathbf{q}_1+\mathbf{q}_2)]+2[\Gamma_{30}(-\mathbf{q}_1-\mathbf{q}_2,\mathbf{q}_1)+\Gamma_{30}(\mathbf{q}_1,-\mathbf{q}_1-\mathbf{q}_2)+\Gamma_{30}(\mathbf{q}_1,\mathbf{q}_2)]W_{12}(\mathbf{q}_1+\mathbf{q}_2)\\
&\times[\Gamma_{32}(\mathbf{q}_3,\mathbf{q}_1+\mathbf{q}_2)+\Gamma_{32}(\mathbf{q}_3,\mathbf{q}_4)]+2\Gamma_{31}(\mathbf{q}_1,\mathbf{q}_2)W_{12}(\mathbf{q}_1+\mathbf{q}_2)[\Gamma_{31}(\mathbf{q}_1+\mathbf{q}_2,\mathbf{q}_3)+\Gamma_{31}(\mathbf{q}_3,\mathbf{q}_1+\mathbf{q}_2)]\\
&+2\Gamma_{31}(\mathbf{q}_1,\mathbf{q}_2)W_{22}(\mathbf{q}_1+\mathbf{q}_2)[\Gamma_{32}(\mathbf{q}_3,\mathbf{q}_1+\mathbf{q}_2)+\Gamma_{32}(\mathbf{q}_3,\mathbf{q}_4)]\},\end{aligned}$$

$$\begin{aligned}\Gamma'_{42}(\mathbf{q}_1,\mathbf{q}_2,\mathbf{q}_3)=&\Gamma_{42}(\mathbf{q}_1,\mathbf{q}_2,\mathbf{q}_3)-\tfrac{1}{3}\{2[\Gamma_{30}(-\mathbf{q}_1-\mathbf{q}_2,\mathbf{q}_1)+\Gamma_{30}(\mathbf{q}_1,-\mathbf{q}_1-\mathbf{q}_2)+\Gamma_{30}(\mathbf{q}_1,\mathbf{q}_2)]W_{11}(\mathbf{q}_1+\mathbf{q}_2)\Gamma_{32}(\mathbf{q}_1+\mathbf{q}_2,\mathbf{q}_3)\\
&+[\Gamma_{31}(\mathbf{q}_1+\mathbf{q}_3,\mathbf{q}_2)+\Gamma_{31}(\mathbf{q}_2,\mathbf{q}_1+\mathbf{q}_3)]W_{11}(\mathbf{q}_1+\mathbf{q}_3)[\Gamma_{31}(-\mathbf{q}_1-\mathbf{q}_3,\mathbf{q}_1)+\Gamma_{31}(\mathbf{q}_1,-\mathbf{q}_1+\mathbf{q}_3)]\\
&+2\Gamma_{31}(\mathbf{q}_1,\mathbf{q}_2)W_{12}(\mathbf{q}_1+\mathbf{q}_2)\Gamma_{32}(\mathbf{q}_1+\mathbf{q}_2,\mathbf{q}_3)+2[\Gamma_{30}(-\mathbf{q}_1-\mathbf{q}_2,\mathbf{q}_1)+\Gamma_{30}(\mathbf{q}_1,-\mathbf{q}_1-\mathbf{q}_2)+\Gamma_{30}(\mathbf{q}_1,\mathbf{q}_2)]\\
&\times W_{12}(\mathbf{q}_1+\mathbf{q}_2)[\Gamma_{33}(\mathbf{q}_1+\mathbf{q}_2,\mathbf{q}_3)+\Gamma_{33}(\mathbf{q}_3,\mathbf{q}_1+\mathbf{q}_2)+\Gamma_{33}(\mathbf{q}_3,\mathbf{q}_4)]+2[\Gamma_{31}(\mathbf{q}_1+\mathbf{q}_3,\mathbf{q}_2)+\Gamma_{31}(\mathbf{q}_2,\mathbf{q}_1+\mathbf{q}_3)]\\
&\times W_{12}(\mathbf{q}_1+\mathbf{q}_3)[\Gamma_{32}(\mathbf{q}_1,-\mathbf{q}_1-\mathbf{q}_3)+\Gamma_{32}(\mathbf{q}_1,\mathbf{q}_3)]+2\Gamma_{31}(\mathbf{q}_1,\mathbf{q}_2)W_{22}(\mathbf{q}_1+\mathbf{q}_2)[\Gamma_{33}(\mathbf{q}_1+\mathbf{q}_2,\mathbf{q}_3)\\
&+\Gamma_{33}(\mathbf{q}_3,\mathbf{q}_1+\mathbf{q}_2)+\Gamma_{33}(\mathbf{q}_3,\mathbf{q}_4)]+[\Gamma_{32}(\mathbf{q}_2,\mathbf{q}_1+\mathbf{q}_3)+\Gamma_{32}(\mathbf{q}_2,\mathbf{q}_4)]W_{22}(\mathbf{q}_1+\mathbf{q}_3)[\Gamma_{32}(\mathbf{q}_1,-\mathbf{q}_1-\mathbf{q}_3)\\
&+\Gamma_{32}(\mathbf{q}_1,\mathbf{q}_3)]\},\end{aligned}$$

$$\begin{aligned}\Gamma'_{43}(\mathbf{q}_1,\mathbf{q}_2,\mathbf{q}_3)=&\Gamma_{43}(\mathbf{q}_1,\mathbf{q}_2,\mathbf{q}_3)-\tfrac{1}{3}\{2\Gamma_{32}(\mathbf{q}_1+\mathbf{q}_2,\mathbf{q}_3)W_{11}(\mathbf{q}_1+\mathbf{q}_2)[\Gamma_{31}(-\mathbf{q}_1-\mathbf{q}_2,\mathbf{q}_1)+\Gamma_{31}(\mathbf{q}_1,-\mathbf{q}_1-\mathbf{q}_2)]+2\Gamma_{32}(\mathbf{q}_1+\mathbf{q}_2,\mathbf{q}_3)\\
&\times W_{12}(\mathbf{q}_1+\mathbf{q}_2)[\Gamma_{32}(\mathbf{q}_1,\mathbf{q}_2)+\Gamma_{32}(\mathbf{q}_1,-\mathbf{q}_1-\mathbf{q}_2)]+2[\Gamma_{31}(-\mathbf{q}_1-\mathbf{q}_2,\mathbf{q}_1)+\Gamma_{31}(\mathbf{q}_1,-\mathbf{q}_1-\mathbf{q}_2)]\\
&\times W_{12}(\mathbf{q}_1+\mathbf{q}_2)[\Gamma_{33}(\mathbf{q}_1+\mathbf{q}_2,\mathbf{q}_3)+\Gamma_{33}(\mathbf{q}_3,\mathbf{q}_1+\mathbf{q}_2)+\Gamma_{33}(\mathbf{q}_3,\mathbf{q}_r)]+2[\Gamma_{32}(\mathbf{q}_1,-\mathbf{q}_1-\mathbf{q}_2)+\Gamma_{32}(\mathbf{q}_1,\mathbf{q}_2)]\\
&\times W_{22}(\mathbf{q}_1+\mathbf{q}_2)[\Gamma_{33}(\mathbf{q}_1+\mathbf{q}_2,\mathbf{q}_3)+\Gamma_{33}(\mathbf{q}_3,\mathbf{q}_1+\mathbf{q}_2)+\Gamma_{33}(\mathbf{q}_3,\mathbf{q}_4)]\},\end{aligned}$$

$$\Gamma'_{44}(\mathbf{q}_1,\mathbf{q}_2,\mathbf{q}_3)=\Gamma_{44}(\mathbf{q}_1,\mathbf{q}_2,\mathbf{q}_3)-\tfrac{1}{3}\{\Gamma_{32}(\mathbf{q}_1+\mathbf{q}_2,\mathbf{q}_3)W_{11}(\mathbf{q}_1+\mathbf{q}_2)\Gamma_{32}(-\mathbf{q}_1-\mathbf{q}_2,\mathbf{q}_1)+2\Gamma_{32}(\mathbf{q}_1+\mathbf{q}_2,\mathbf{q}_3)W_{12}(\mathbf{q}_1+\mathbf{q}_2)$$
$$\times[\Gamma_{33}(-\mathbf{q}_1-\mathbf{q}_2,\mathbf{q}_1)+\Gamma_{33}(\mathbf{q}_1,-\mathbf{q}_1-\mathbf{q}_2)+\Gamma_{33}(\mathbf{q}_1,\mathbf{q}_2)]+[\Gamma_{33}(-\mathbf{q}_1-\mathbf{q}_2,\mathbf{q}_1)+\Gamma_{33}(\mathbf{q}_1,-\mathbf{q}_1-\mathbf{q}_2)$$
$$+\Gamma_{33}(\mathbf{q}_1,\mathbf{q}_2)]W_{22}(\mathbf{q}_1+\mathbf{q}_2)[\Gamma_{33}(\mathbf{q}_1+\mathbf{q}_2,\mathbf{q}_3)+\Gamma_{33}(\mathbf{q}_3,\mathbf{q}_1+\mathbf{q}_2)+\Gamma_{33}(\mathbf{q}_3,\mathbf{q}_4)]\}, \tag{A18}$$

where $\mathbf{q}_4=-\mathbf{q}_1-\mathbf{q}_2-\mathbf{q}_3$.

APPENDIX B

To calculate $\langle Q_n\rangle$ in Eq. (A5), the expansion of the partition function $\langle Q\rangle$ to the n-th power in the conjugate fields, we should count all the combinations of $\gamma_A^i\gamma_B^{n-i}$ ($i=0$ to n) as additive terms (e.g., all the Γ_{4i} terms in $\langle Q_4\rangle$). For one specific component such as $\Gamma_{42}(\mathbf{q}_1,\mathbf{q}_2,\mathbf{q}_3)\gamma_A(\mathbf{q}_1)\times\gamma_A(\mathbf{q}_2)\gamma_B(\mathbf{q}_3)\gamma_B(-\mathbf{q}_1-\mathbf{q}_2-\mathbf{q}_3)$, there are several contributions to the coefficient Γ_{42} coming from the permutations of all the possible positions of the conjugate fields. Each such contribution contains integrals of the positions of every segment of the chain. In order to simplify the counting and evaluation of these integrals, as well as to clarify the angular dependence of the $\mathbf{q}_i$'s, we introduce a graphical method. The rules which describe this method are as follows:

- A graph is composed of propagators, external lines, internal points, and blobs (external points), see Fig. 10.
- Each propagator starts and ends at an internal point or a blob, respectively; one wave vector $\mathbf{q}$, a starting index, and an ending index are associated with one propagator.

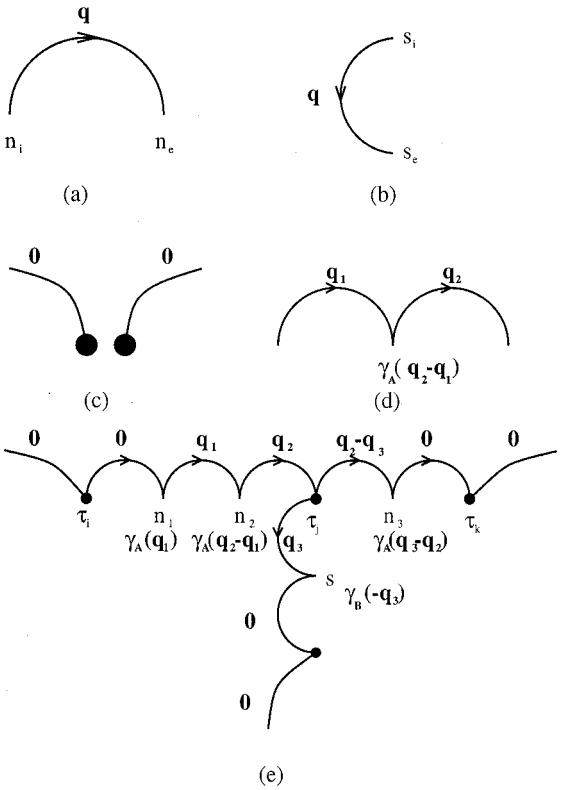

FIG. 10. Components of a graph are shown in (a)–(d): Internal points and a propagator (a) for the backbone and (b) for a branch; (c) external lines and blobs; (d) an internal point and its associated conjugate field. An example of one term in $\langle Q_4\rangle$ is shown in (e).

A factor equal to $\exp[-x(n_e-n_i)]$ for a backbone propagator or equal to $\exp[-x(s_e^j-s_i^j)]$ for a jth branch propagator is multipled into the corresponding term of the partition function. Here $x=q^2b^2/6$, n_e, n_i and s_e^j, s_i^j are the ending and starting index of monomer on the backbone and the jth branch, respectively. The direction of the propagator is defined such that for the backbone it is from the first to the Nth monomer, for a branch it is from the branch point to the branch end. See Figs. 10(a) and 10(b).

- A branch starts from a blob, and an index counting both the branches and the position on the backbone (e.g., τ_i, where i means the i-th branch on the backbone) is associated with a blob. Each external line either starts at a blob with no end or ends at a blob with no beginning, and $\mathbf{q}=0$ is associated with the external line. See Fig. 10(c).
- For each internal point of the backbone, a conjugated field $\gamma_A(\mathbf{q}_2-\mathbf{q}_1)$ is associated; for each internal point of a branch, a conjugated field $\gamma_B(\mathbf{q}_2-\mathbf{q}_1)$ is associated. Here $\mathbf{q}_1$ and $\mathbf{q}_2$ are the wave vectors associated with the incoming and outcoming propagators of this internal point. See Fig. 10(d).
- For each blob, we ensure momentum conservation for the wave vectors connected to the blob.
- All explicit $\mathbf{q}$'s are integrated; all the indices for internal points and blobs are integrated or summed up (notice: no permutation for these indices).
- A prefactor of $-i$, or $-\frac{1}{2}$, or $i/6$, or $1/24$ is associated with a single internal point, or a double internal point, or a triple internal point, or a quadruple internal point, respectively.

A typical term in $\langle Q_4\rangle$ is shown in Fig. 10(e). As the rules point out, this graph is equal to

$$(-i)(-i)\left(\frac{-1}{2}\right)\left\langle\sum_{i<j<k}^{P}\int d\mathbf{q}_1\,d\mathbf{q}_2\,d\mathbf{q}_3\right.$$
$$\times\int_{\tau_i}^{\tau_j}dn_2\int_{\tau_i}^{n_2}dn_1\int_{\tau_j}^{\tau_k}dn_3\int_0^M ds\,\gamma_A(\mathbf{q}_1)\gamma_A(\mathbf{q}_2-\mathbf{q}_1)$$
$$\times\gamma_A(\mathbf{q}_3-\mathbf{q}_2)\gamma_B(-\mathbf{q}_3)\exp[-x_1|n_2-n_1|]$$
$$\left.\times\exp[-x_2|\tau_j-n_2|]\exp[-x_3s]\exp[-x4|n_3-\tau_j|]\right\rangle, \tag{B1}$$

where $x_i=q_i^2b^2/6$ for $i=1$, 2, 3 and $x_4=(\mathbf{q}_3-\mathbf{q}_2)^2b^2/6$. By permuting the position of branch (j) and the three internal points (n_1, n_2, and n_3), we get other contributions to $\Gamma_{41}\gamma_A^3\gamma_B$. As an example, we show all the contributions to $\Gamma_{43}\gamma_A\gamma_B^3$ in Fig. 11.

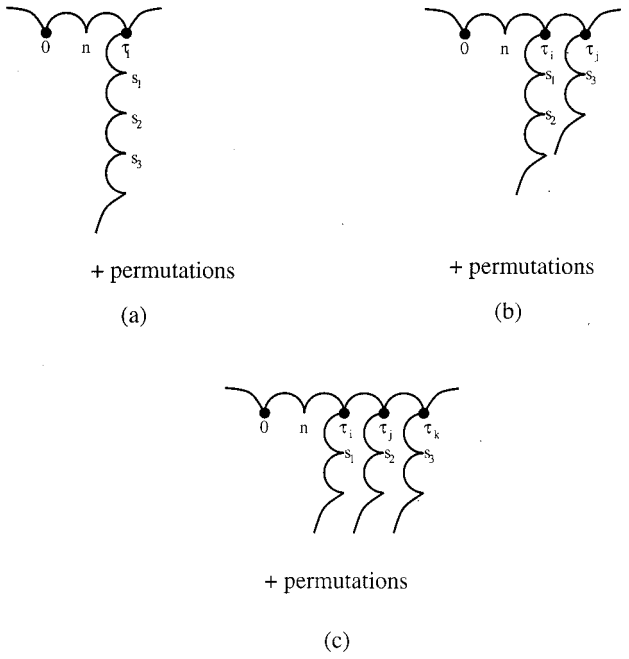

FIG. 11. All the terms that contribute to $\Gamma_{43}\gamma_A\gamma_B^3$ are shown in (a)–(c). The permutation operates on all the s_i's and τ_i's.

As a simple example, we apply this method to a homopolymer chain with N monomers. The quadratic term is show in Fig. 12(a), and the corresponding quadratic term is:

$$-\frac{1}{2}\int d\mathbf{q}\gamma(\mathbf{q})\gamma(-\mathbf{q})\int_0^N dn_1\,dn_2\exp[-x|n_2-n_1|]$$

$$=-\frac{1}{2}\int d\mathbf{q}\gamma(\mathbf{q})\gamma(-\mathbf{q})N^2g_2(Nx), \tag{B2}$$

where $x=q^2b^2/6$. The quartic term is shown in Fig. 12(b), with the corresponding expression being

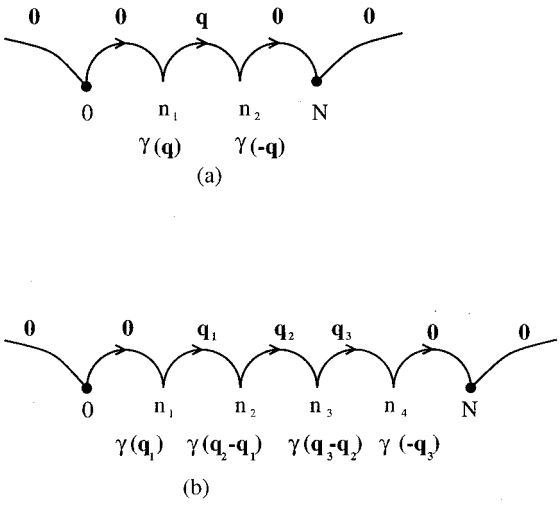

FIG. 12. The graphs of (a) the quadratic term and (b) the quartic term for a homopolymer chain.

$$\frac{1}{24}\int d\mathbf{q}_1\,d\mathbf{q}_2\,d\mathbf{q}_3\gamma(\mathbf{q}_1)\gamma(\mathbf{q}_2-\mathbf{q}_1)\gamma(\mathbf{q}_3-\mathbf{q}_2)\gamma(-\mathbf{q}_3)$$
$$\times\int_0^N dn_1\,dn_2\,dn_3\,dn_4\exp[-x_1|n_2-n_1|]$$
$$\times\exp[-x_2|n_3-n_2|]\exp[-x_3|n_4-n_3|]$$
$$=\ d\mathbf{q}1\,d\mathbf{q}2\,d\mathbf{q}3\gamma(\mathbf{q}1)\gamma(\mathbf{q}2-\mathbf{q}1)\gamma(\mathbf{q}3-\mathbf{q}2)$$
$$\times\gamma(-\mathbf{q}_3)N^4H_3(Nx_1,Nx_2,Nx_3), \tag{B3}$$

where $x_i=q_i^2b^2/6$ for $i=1, 2, 3$.

APPENDIX C

After we obtain the expression for these graphs [e.g., Eq. (B1)], the next step is to calculate the quenched average over τ_j. To do this, we introduce the parameter $\alpha_i=\theta_i-\overline{\theta_i}$ $(i=A,B)$, where $\theta_A=1$, $\theta_B=-1$ and $\overline{\theta_i}=(2f_A-1)$ $(f_A=(N-P)/N=1-f_B$ is the fraction of segments of type-A on the backbone). Thus $\alpha_A=2f_B$ and $\alpha_B=-2f_A$. It is easy to show that α_i satisfy

$$\begin{aligned}
&\langle\alpha_i\rangle=0,\\
&\langle\alpha_i\alpha_j\rangle=4f_Af_B\delta_{ij},\\
&\langle\alpha_i\alpha_j\alpha_k\rangle=8(f_Af_B^2-f_A^2f_B)\delta_{ijk},\\
&\langle\alpha_i\alpha_j\alpha_k\alpha_l\rangle=16f_A^2f_B^2(\delta_{ij}\delta_{kl}+\delta_{ik}\delta_{jl}+\delta_{il}\delta_{jk})\\
&\qquad\qquad+48f_Af_B(f_B-f_A)^2\delta_{ijkl}.
\end{aligned} \tag{C1}$$

The rule to perform the quenched average of a typical term like that in Eq. (B1) is: for each summation subscript (j) for the branch position (τ_j), introduce a factor $(f_B-\alpha_j/2)$, also change τ_j to j, and change the summation of $\Sigma_{j=1}$ to $\int_{j=0}dj$. For example, Eq. (B1) is changed to

$$\frac{1}{2}\int_0^N dk\int_0^\sigma dj\int_0^j di\int d\mathbf{q}_1\,d\mathbf{q}_2\,d\mathbf{q}_3$$
$$\times\int_i^j dn_1\,dn_2\int_j^k dn_3\int_0^M ds\,\gamma_A(\mathbf{q}_1)\gamma_A(\mathbf{q}_2-\mathbf{q}_1)\gamma_A(\mathbf{q}_3-\mathbf{q}_2)$$
$$\times\gamma_B(-\mathbf{q}_3)\exp[-x_1|n_2-n_1|]\exp[-x_2|j-n_2|]$$
$$\times\exp[-x_3s]\exp[-x^4|n_3-j|]$$
$$\times\left\langle\left(f_B-\frac{\alpha_i}{2}\right)\left(f_B-\frac{\alpha_j}{2}\right)\left(f_B-\frac{\alpha_k}{2}\right)\right\rangle. \tag{C2}$$

Thus the average over the positions τ_j is transferred to an average over the parameters α_j. It is easy to see that this transformation is performed such that when monomer A is the jth monomer on the backbone, $[f_B-(\alpha_j/2)]=0$, then there is no contribution to the sum; when monomer B is the jth monomer on the backbone, $[f_B-(\alpha_j/2)]=1$, there is contribution to the sum with weight 1. Therefore, it is equivalent to the original summation over τ_j.

[1] L. Leibler, Macromolecules **13**, 1602 (1980).
[2] F. S. Bates and G. H. Fredrickson, Annu. Rev. Phys. Chem. **41**, 525 (1990); G. H. Fredrickson and F. S. Bates, Annu. Rev. Mater. Sci. **26**, 501 (1996).

[3] A. Sali, E. I. Shakhnovich, and M. Karplus, Nature (London) **369**, 248 (1994).
[4] H. Frauenfelder and P. G. Wolynes, Phys. Today **47**, 57 (1994).
[5] H. S. Chan and K. A. Dill, Phys. Today **46**, 24 (1993).
[6] D. Bratko, A. K. Chakraborty, and E. I. Shakhnovich, Phys. Rev. Lett. **76**, 1844 (1996).
[7] S. Srebnik, A. K. Chakraborty, and E. I. Shakhnovich, Phys. Rev. Lett. **77**, 3157 (1996).
[8] E. I. Shakhnovich and A. M. Gutin, J. Phys. (Paris) **50**, 1843 (1989).
[9] G. H. Fredrickson and S. T. Milner, Phys. Rev. Lett. **67**, 835 (1991); G. H. Fredrickson, S. T. Milner, and L. Leibler, Macromolecules **25**, 6341 (1992).
[10] A. M. Gutin, A. Yu. Grosberg, and E. I. Shakhnovich, Macromolecules **26**, 3598 (1993).
[11] A. Shinozaki, D. Jasnow, and A. C. Balazs, Macromolecules **27**, 2496 (1994).
[12] A. Werner and G. H. Fredrickson, J. Polym. Sci., Part B: Polym. Phys. **35**, 849 (1997).
[13] M. Xenidou and N. Hadjichristidis, Macromolecules **31**, 5690 (1998).
[14] S. Qi, A. K. Chakraborty, H. Wang, A. A. Lefebvre, N. P. Balsara, E. I. Shakhnovich, M. Xenidou, and N. Hadjichristidis, Phys. Rev. Lett. **82**, 2896 (1999).
[15] S. F. Edwards and P. W. Anderson, J. Phys. (Paris) **5**, 965 (1975).
[16] K. M. Hong and J. Noolandi, Macromolecules **14**, 727 (1981).
[17] A. Mayes and M. O. de la Cruz, Macromolecules **24**, 3975 (1991); H. Tang and K. Freed, J. Chem. Phys. **96**, 8621 (1992); M. O. de la Cruz, Phys. Rev. Lett. **67**, 85 (1991); K. R. Shull, Macromolecules **25**, 2122 (1992); J. L. Barrat and G. H. Fredrickson, J. Chem. Phys. **95**, 1281 (1991); K. Almdal, J. H. Rosedale, F. S. Bates, G. D. Wignall, and G. H. Fredrickson, Phys. Rev. Lett. **65**, 1112 (1990).
[18] S. V. Panyukov and I. I. Potemkin, JETP Lett. **64**, 197 (1996); S. V. Panyukov and I. I. Potemkin, JETP **85**, 183 (1997); *ibid.* **85**, 183 (1997); I. I. Potemkin and S. V. Panyukov, Phys. Rev. E **57**, 6902 (1998); S. V. Panyukov and I. I. Potemkin, Phys. A **249**, 321 (1998).
[19] A. Nesarikar, M. O. de la Cruz, and B. Crist, J. Chem. Phys. **98**, 7385 (1993).
[20] A. V. Dobrynin and L. Leibler, Europhys. Lett. **36**, 283 (1996); A. V. Dobrynin, J. Chem. Phys. **107**, 9234 (1997).
[21] H. J. Angerman, G. tenBrinke, and I. Erukhimovich, Macromolecules **29**, 3255 (1996); *ibid.* **31**, 1958 (1998); H. J. Angerman, G. tenBrinke, and J. J. M. Slot, Euro. Phys. Journ. B **12**, 397 (1999).
[22] N. P. Balsara, B. A. Garetz, and H. J. Dai, Macromolecules **25**, 6072 (1992); C. C. Lin, S. V. Jonnalagadda, P. K. Kesani, H. J. Dai, and N. P. Balsara, *ibid.* **27**, 7769 (1994).
[23] L. J. Fetters *et al.*, *Physical Properties of Polymers Handbook*, edited by J. E. Mark (AIP, Woodbury, NY, 1996), Chap. 24.